Anion Binding and Controlled Aggregation of Human Interleukin-1 Receptor Antagonist

ARTICLE *in* BIOCHEMISTRY · AUGUST 2005

Impact Factor: 3.02 · DOI: 10.1021/bi050388g · Source: PubMed

6 AUTHORS, INCLUDING:

Andrei Raibekas
Neurozon LLC
25 PUBLICATIONS **1,168** CITATIONS
SEE PROFILE

Ramil F Latypov
Amgen
36 PUBLICATIONS **645** CITATIONS
SEE PROFILE

Bruce A Kerwin
Amgen
46 PUBLICATIONS **1,291** CITATIONS
SEE PROFILE

Anion Binding and Controlled Aggregation of Human Interleukin-1 Receptor Antagonist

Andrei A. Raibekas,*,‡ Edward J. Bures,‡ Christine C. Siska,‡ Tadahiko Kohno,§ Ramil F. Latypov,‡ and Bruce A. Kerwin‡

Departments of Pharmaceutics and Protein Science, Amgen Inc., One Amgen Center Drive, Thousand Oaks, California 91320

Received March 1, 2005; Revised Manuscript Received May 15, 2005

ABSTRACT: Highly concentrated human recombinant interleukin-1 receptor antagonist (IL-1ra) aggregates at elevated temperature without perturbation in its secondary structure. The protein aggregation can be suppressed depending on the buffer ionic strength and the type of anion present in the sample solution. Phosphate is an approximately 4-fold weaker suppressant than either citrate or pyrophosphate on the basis of the measured protein aggregation rates. This is in agreement with the strength of protein−anion interactions at the IL-1ra single anion-binding site as judged by the estimated dissociation constant values of 2.9 mM, 3.8 mM, and 13.7 mM for pyrophosphate, citrate, and phosphate, respectively. The strength of binding also correlates with the anion size and with the number of ionized groups available per molecule at a given pH. Affinity probing of IL-1ra with methyl acetyl phosphate (MAP) in combination with proteolytic digestion and mass spectral analysis show that an anion-binding site location on the IL-1ra surface is contributed by lysine-93 and lysine-96 of the loop 84−98 as well as by lysine-6 of the unstructured N-terminal region 1−7. The replacement of lysine-93 with alanine by site-directed mutagenesis results in dramatically suppressed IL-1ra aggregation. Furthermore, when the unstructured N-terminal region of IL-1ra is removed by limited proteolysis, a 2-fold increase in the time course of the aggregation lag phase is observed for the truncated protein. An anion-controlled mechanism of IL-1ra aggregation is proposed by which the anion competition for the protein cationic site prevents formation of intermolecular cation−π interactions and, thus, interferes with the protein asymmetric self-association pathway.

The detailed understanding of protein aggregation is an essential task not only from a fundamental prospective but also when considering the role that aggregated species, such as amyloid plaques and Lewy bodies, play in certain diseases. Consequently, it can provide guidance to develop the corresponding therapeutic strategies (*1*). It has been previously observed that proteins with predominant β-strand secondary structure are generally prone to aggregation. For example, the fibroblast growth factor (FGF) family of proteins such as acidic and basic fibroblast growth factors as well as keratinocyte growth factor (KGF) share the same β-barrel structural fold and are known to aggregate at elevated temperatures (*2*−*5*). Moreover, both α-synuclein and myoglobin can adopt non-native β-sheet secondary structure and, consequently, promote self-aggregation into a fibrillar species (*6*−*8*). Earlier theoretical model studies suggested that the aggregation kinetic process could be essentially separated into a thermodynamically unfavorable nucleation phase followed by a growth phase with a corresponding decrease in the free energy of the system (*9*, *10*). In certain cases, the aggregation has been linked to protein structural rearrangements and can be influenced by a variety of factors such as protein concentration, hydrophobicity, ionic strength, temperature, and the presence of metals and multi-ions (*11*−*14*). Still, the molecular mechanisms, pathways of protein aggregation, and, more specifically, the influence of ions or electrostatic protein−ion interactions on the protein aggregation process (*3*, *14*) are poorly understood.

Herein we describe the effect of a series of anions on aggregation of the interleukin-1 receptor antagonist (IL-1ra)[1] at elevated temperature and attribute it primarily to anion charge properties at a given pH. We also obtain evidence for the contribution of the single protein anion-binding site as a modulator of the IL-1ra aggregation process and attempt to map the location of this site by using a dual-mode affinity probe, methyl acetyl phosphate (MAP).

Human interleukin-1 receptor antagonist is a 17-kDa member of the IL-1/FGF family of proteins and a naturally occurring IL-1 blocker that plays an important regulatory role in inflammation and functioning of the adaptive immune system (*15*). The β-trefoil topology (*16*) is a characteristic structural feature of IL-1ra and its family. In the case of IL-1ra, it consists of twelve antiparallel β-strands, six of which are arranged in the form of a β-barrel end-closed by another six β-strands (*17*−*19*).

MATERIALS AND METHODS

Purified recombinant human interleukin-1 receptor antagonist (IL-1ra) was supplied by Amgen manufacturing

* To whom correspondence should be addressed. E-mail: andreir@amgen.com. Phone: (805) 447-5763. Fax: (805) 376-8505.
‡ Department of Pharmaceutics.
§ Department of Protein Science.

[1] Abbreviations: IL-1ra, interleukin-1 receptor antagonist; MAP, methyl acetyl phosphate; MS, mass spectrometry; LC−MS/MS, liquid chromatography tandem mass spectrometry; CD, circular dichroism; HPLC, high-performance liquid chromatography.

10.1021/bi050388g CCC: $30.25
Published on Web 06/30/2005

facility. Endoproteinase Lys-C (sequencing grade) was purchased from Roche Diagnostics (Indianapolis, IN). All other chemicals were of the highest grade available.

Aggregation Assay. IL-1ra aggregation in phosphate buffer and citrate buffer was conducted as follows. Usually, 10 mL of IL-1ra stock solution (200−220 mg/mL protein in 10 mM sodium citrate, 140 mM NaCl, 0.5 mM EDTA, pH 6.5 (CSE buffer)) was dialyzed overnight at 4 °C against either 2 × 2 L of 10 mM sodium phosphate, 140 mM NaCl, 0.5 mM EDTA, pH 6.5 (PSE buffer) or 2 × 2 L of CSE. The dialyzed solution was filtered through a 0.2 μm filter, and the protein concentration was adjusted to 100−140 mg/mL by diluting with the appropriate buffer. The protein concentration was estimated by its absorbance at 279 nm using an Agilent 8453 spectrophotometer and the extinction coefficient of 13392 M^{-1} cm^{-1}. The latter was derived on the basis of the protein absorbance at 279 nm and the corresponding protein concentration determined using a Beckman 6300 amino acid analyzer. Aggregation of IL-1ra in each buffer was measured using a 96-well glass plate (Alltech, Deerfield, IL) and a temperature-controlled plate reading spectrophotometer, SpectraMax Plus (Molecular Devices, Sunnyvale, CA). The sample volume per well was 180 μL. The plates were incubated in the spectrophotometer at 40 °C, and the optical density was measured at 405 nm with 1-min intervals and a 3-s automated shaking step between readings. To estimate corresponding amounts of the aggregated protein, the experiment was set up as described above; samples were withdrawn at different time points of incubation (40 °C) and immediately placed in 1.5-mL centrifuge tubes on ice. For each sample, the aggregated material was collected in a 1.5-mL tube by centrifugation (13000*g*, 30 min) at 10 °C using a Beckman Coulter Microfuge 22R centrifuge, the pellet was washed with 0.2 mL of cold deionized water, centrifuged (13000*g*, 30 min), and redissolved in 180 μL of freshly prepared 30 mM sodium phosphate buffer, pH 7.0, containing 6 M urea (room temperature), and the protein concentration was measured by its absorbance at 279 nm in the same buffer.

The rate of aggregation was determined as the slope of the linear growth region of the saturation curve and defined as ΔOD per hour per mole of protein. The rate of aggregation of IL-1ra was also determined in different buffer compositions with increasing ionic strength. Aliquots of the dialyzed IL-1ra solution (in 10 mM phosphate buffer, pH 6.5, containing 80 mM NaCl) were brought to various concentrations of citrate, phosphate, or pyrophosphate using 0.45−0.5 M citrate, phosphate, or pyrophosphate stock solutions (all pH 6.5) and an appropriate volume of 80 mM NaCl to result in a final concentration of IL-1ra in each sample of 140 mg/mL. The relative concentration of added citrate, phosphate, or pyrophosphate in each sample ranged from 1 to 200 mM. Aggregation of IL-1ra in each sample was monitored for 4 h at 39 °C by measuring the optical density at 405 nm as described above.

Citrate Binding and Competition Assays. The number of citrate ion binding sites and the dissociation constant (K_d) value for citrate binding to IL-1ra were estimated as follows. Solutions of 1 mL of 1 mM IL-1ra were prepared in buffers having various concentrations of citrate, pH 6.5 by diluting IL-1ra stock (220 mg/mL in CSE) in appropriate buffers. Specifically, 1-mL volumes of 1 mM solutions of IL-1ra in 0−20 mM citrate, pH 6.5 were prepared. Each solution also contained 70 mM NaCl. The 0.6-mL aliquot of each sample solution was placed in a corresponding Microsep-10 ultrafiltration spin unit (Pall Life Sciences, Ann Arbor, MI) and was centrifuged at 18 °C for 35 min at 4000*g* to achieve an equal distribution of volume (2 × 0.3 mL) between retentate and filtrate. To determine citrate concentration using its absorbance at 215 nm, 20 μL of filtrate or retentate was loaded onto a reverse-phase HPLC column (Supelcosil LC-18 column, 15 cm × 4.6 mm, Sigma-Aldrich). The flow rate was 1 mL/min with 0.1 M phosphoric acid as a mobile phase. Isocratic elution was carried out at room temperature, and the eluent absorbance was monitored at 215 nm. The concentration of citrate in the sample being assayed (i.e., retentate or filtrate) was calculated on the basis of a calibration curve of 0−10 mM citrate standard solutions, pH 6.5. The amount of bound citrate was calculated on the basis of the difference between its retentate and filtrate values.

Competition experiments were conducted in a similar fashion as above, except they were done in the presence of 10 mM citrate, 70 mM NaCl, pH 6.5 and increased (0−20 mM) concentrations of phosphate or pyrophosphate, pH 6.5. The dissociation constants for competitive binding were calculated according to Stinson and Holbrook (*20*). The apparent dissociation constant for citrate binding to IL-1ra was estimated in the presence of increased concentrations of competitive anion and then plotted against the corresponding values of free (unbound) competitive anion. The latter was calculated from the total concentration of competitive anion minus the relative decrease (ΔPL) in the concentration of bound ligand (citrate) as the total concentration of competitive anion is increased, i.e., $X(f) = X(t) - \Delta PL$. The plot data were linear fitted, and K_d values for competitive anion binding were calculated from the resulting linear curve as equal to the *y*-axis intercept value of the curve divided by its slope value.

Derivatization of IL-1ra with Methyl Acetyl Phosphate. Methyl acetyl phosphate (MAP) was prepared as described by Kluger and Tsui (*21*). The identity of the product was confirmed by NMR and mass spectrometry. IL-1ra was reacted with MAP in the presence of citrate, phosphate, or pyrophosphate as follows. For the derivatization in the presence of citrate, 20 μL of MAP (10 mM stock in water) and 20 μL of IL-1ra (1 mM stock in CSE) were added to 160 μL of 10 mM buffer, pH 6.5 in an HPLC vial. The reaction mixture was incubated at 37 °C, and 25-μL aliquots were automatically withdrawn for analysis within the first 5.5 h of incubation. Each aliquot was analyzed using an Agilent 110 HPLC system equipped with a Jupiter 5μ C4 300 Å reverse-phase HPLC column (4.6 × 250 mm, Phenomenex, Torrance, CA), an on-line UV detector, and a temperature-controlled 100-well sample tray set at 37 °C. The flow rate was set at 1 mL/min, and the column was maintained at a temperature of 50 °C. The column was preequilibrated for 15 min (flow rate 1 mL/min) with 65% buffer A (0.1% trifluoroacetic acid (TFA) in water) and 35% buffer B (90% acetonitrile, 0.1% TFA in water). After loading, the analytes were eluted using a gradient ramping from 35% to 50% buffer B over 25 min. The same protocol was applied for reactions of MAP with IL-1ra in the presence of phosphate and pyrophosphate. The reaction products separated by reverse-phase HPLC were further analyzed in order to determine the reactive sites, as follows. The

separated peak fractions were collected and concentrated on a SpeedVac vacuum concentrator to 5−10 μL final volume, and then 90 μL of digest buffer (50 mM Tris HCl, 0.8 M guanidinium-HCl, pH 8.0) was added to each sample followed by 10 μL of endoproteinase Lys-C (1 μg in 10 μL of digest buffer). Samples were incubated at 37 °C for 16 h, and the resulting peptides were analyzed by LC−MS/MS using an Agilent 1100 HPLC system equipped with an on-line MS detector (Deca ion trap mass spectrometer, Finnigan, San Jose, CA). The column used was a Jupiter 5μ C18 100 Å reverse-phase HPLC column (2 × 150 mm, Phenomenex, Torrance, CA). The flow rate was set at 0.2 mL/min, and the column was maintained at a temperature of 50 °C. The column was preequilibrated for 22 min with 98% buffer A (0.1% TFA in water) and 2% buffer B (90% acetonitrile, 0.1% TFA in water). After loading, analytes were eluted from the column using a gradient ramping from 2% to 45% buffer B over 50 min. Ten percent of the eluent from the HPLC column was diverted for the on-line MS analysis.

N-Terminal Truncation by Limited Proteolysis. One milliliter of 1 mM protein solution in CSE buffer (10 mM citrate, 140 mM NaCl, 0.5 mM EDTA, pH 6.5) was mixed with 8 μL of a 25 μg/mL solution of endoproteinase Lys-C in CSE buffer. The reaction mixture was incubated for 48 h at 37 °C; the resulting two reaction products, i.e., truncated protein and peptide, were isolated using reverse-phase HPLC conditions as described for Lys-C digests in the previous section and subjected to identification by N-terminal sequence and mass spectral analyses. For aggregation kinetic studies, the reaction solution (after 48 h incubation at 37 °C) was dialyzed overnight at 4 °C against CSE or PSE buffers and subjected to an aggregation assay at 42 °C.

Site-Directed Mutagenesis. The IL-1ra Lys-93 → Ala (K93A) mutation required a triple-base substitution (AAA → GCT) in wild-type protein polynucleotide encoding sequence inserted into pAMG21 vector (ATCC No. 98113) at *Nde*I and *Hin*dIII sites (referred to as pAMG21-WT) and was performed on pAMG21-WT according to a PCR-based method described by Horton et al. (*22*). The resulting PCR amplification product containing IL-1ra encoding sequence and targeted nucleotide substitution was digested with *Nde*I and *Hin*dIII enzymes and ligated into pAMG21 vector precut with the same pair of restriction enzymes to generate a plasmid referred to as pAMG21-K93A. The plasmid was transformed into *Escherichia coli* strain 2596 as an expression host; the transformed cells were grown at 37 °C in Luria broth (LB) media to an optical density (OD_{600}) of 1.0 and then stored at −80 °C in 1-mL aliquots in LB media containing 17% glycerol. The presence of K93A mutation was verified by pAMG21-K93A plasmid DNA sequence analysis.

Protein Expression and Purification. Briefly, K93A IL-1ra was expressed and isolated as follows. Cells were grown at 37 °C in 10.5 L of LB media until an $OD_{600} \sim 9.5$, and then protein expression was induced by addition of 10 mL of 0.5 mg/mL *N*-(3-oxohexanoyl) homoserine lactone followed by another 6 h of cell growth. Cells were harvested by centrifugation, resuspended in 300 mL of cold buffer A (25 mM sodium acetate, pH 5.2, 100 mM NaCl, 1 mM EDTA), and disrupted by sonication. After sonication, the free-cell extract was cleared by centrifugation and loaded onto a Pharmacia SP Sepharose column (2.5 mm × 8 cm)

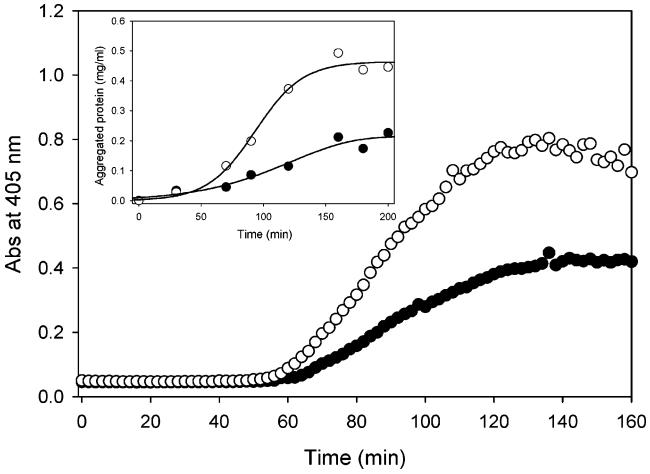

FIGURE 1: Kinetics of thermally induced aggregation of 107 mg/mL IL-1ra measured at 405 nm and 40 °C in 10 mM phosphate (open circles) or 10 mM citrate (filled circles) buffers, pH 6.5, containing 140 mM NaCl and 0.5 mM EDTA. Inset shows a quantitative estimate of the aggregated protein obtained under the above conditions and during incubation at 40 °C (see Materials and Methods for details). Open and filled circles indicate samples containing phosphate and citrate buffers, respectively.

preequilibrated with buffer A. After the column was washed with 2 column volumes of buffer A, the elution was conducted with a 0.1−0.28 M linear gradient of NaCl followed by 3.5 column volumes of buffer B (25 mM sodium acetate, pH 5.2, 280 mM NaCl, 1 mM EDTA). Protein peak fractions were pooled, concentrated to about a 40-mL volume using Ultracell YM10 stirred cell (Millipore, Bedford, MA), dialyzed against buffer C (10 mM histidine, pH 6.0, 50 mM NaCl, 0.1 mM EDTA), and centrifuged (10000 rpm, 30 min). The resulting supernatant was loaded onto a Pharmacia Q Sepharose column (2.5 × 6 cm) preequilibrated with buffer C. After the column was washed with 2 column volumes of buffer C, the protein elution was conducted with a 0.1−0.2 M linear gradient of NaCl. The K93A IL-1ra eluted fractions were pooled, sequentially concentrated with an Amicon Ultracell YM10 stirred cell and Centricon YM10 unit (Millipore) to nearly 100 mg/mL protein concentration, dialyzed overnight at 4 °C against CSE or PSE buffer, and stored at 4 °C prior to further use.

Circular Dichroism. Circular dichroism measurements were performed on an Aviv spectropolarimeter, model 202-01 DS (Aviv Biomedical, Lakewood, NJ). Temperature denaturation experiments were performed in 10−50 mM sodium phosphate buffer, pH 7 and 0−0.5 M final concentration of NaCl. Protein concentration was varied from 5 to 50 μM (0.09 to 0.9 mg/mL, respectively). The temperature range was from 20 °C to 85 °C. Sample solutions were equilibrated for 30 s at every given temperature, with 1 °C step. CD signal was averaged for 30 s. A 2−3 nm bandwidth and 0.2−1 cm path cuvette were typically used.

RESULTS

Anion Dependence of IL-1ra Aggregation. The aggregation of the highly concentrated IL-1ra was monitored at 39−40 °C by the absorbance/light scattering technique described in Materials and Methods, and a typical kinetic profile is shown in Figure 1. Three major phases were observed during this process, i.e., prolonged 40-min lag phase sequentially

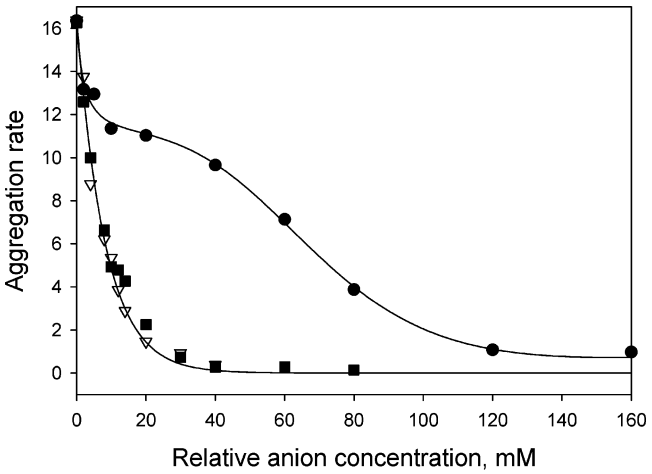

FIGURE 2: Anion dependence of IL-1ra aggregation rates measured at pH 6.5 and 39 °C in the presence of 80 mM NaCl and increased concentrations of phosphate (filled circles), citrate (filled squares), and pyrophosphate (open triangles). Protein concentration is 140 mg/mL. Aggregation rate is defined as ΔOD_{405} per hour per mole of protein.

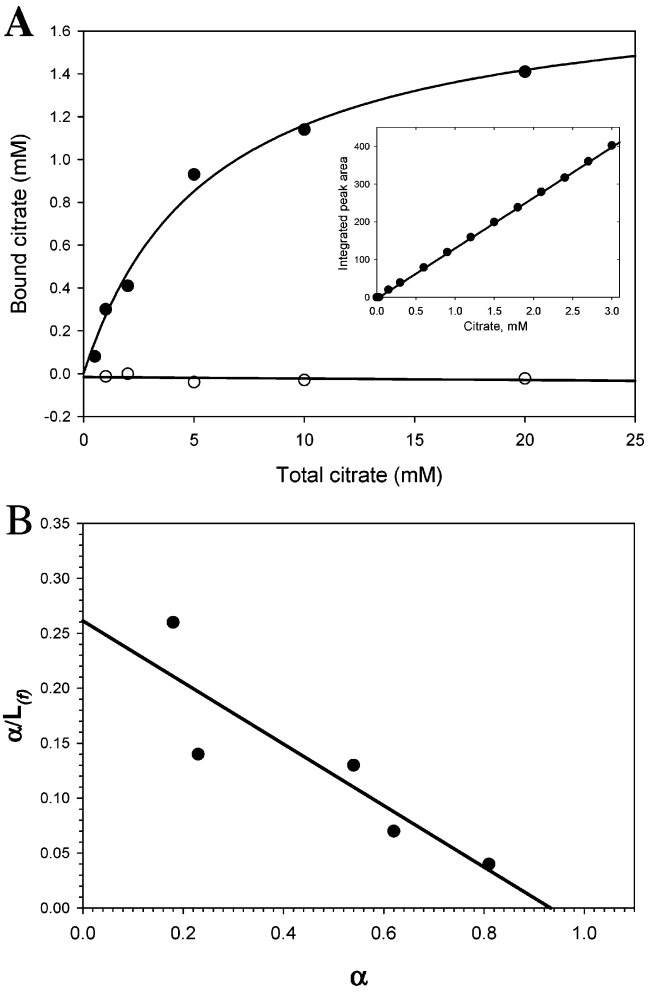

FIGURE 3: Citrate−IL-1ra binding data analysis. (A) Estimated amounts of bound citrate are plotted against correspondingly increased concentrations of total citrate present in the protein sample solution (filled circles). The data are fitted into one binding site saturation curve. Control data plot is shown in open circles. Inset shows citrate standard calibration curve. (B) Scatchard plot derived from the citrate binding data. The *x*-axis intercept indicates one binding site whereas the *y*-axis intercept provides a $1/K_d$ value of 0.26.

followed by phases of linear growth and then saturation (plateau). As seen in Figure 1, there was a striking difference between aggregation growth and saturation phases of IL-1ra sample solutions containing either phosphate or citrate buffers. The aggregation kinetics measured by an increase in optical density directly reflected the accumulation of the aggregated protein (Figure 1, inset). The endpoint fraction of the aggregated protein (plateau level) corresponded to about 0.2% and 0.4% of the initial, soluble protein in samples containing citrate and phosphate buffers, respectively. Moreover, the plateau level correlated with the slope of the linear growth phase, i.e., with the rate of aggregation. It was evident that, under the same experimental and sample conditions (buffer composition, pH, protein concentration, etc.) with exception for phosphate anion being substituted with citrate anion, the latter had an about 50% greater ability to suppress aggregation of IL-1ra. In the next step, the observed aggregation rates were measured at 39 °C using the buffered protein solution, pH 6.5 containing additional, various concentrations of either citrate, phosphate, or pyrophosphate (see Materials and Methods for details). The choice of pyrophosphate was driven by its similarity with citrate as will be discussed below. The citrate and pyrophosphate had a similar effect, generating a sharp decline in the protein aggregation rate within the 0−20 mM concentration range, and, in both cases, the aggregation was close to a zero background level after the anion concentration reached 40 mM (Figure 2). In contrast, the phosphate anion displayed a weaker suppressive nature. At 40 mM concentration, the observed aggregation rate was only 40% reduced versus 98−99% reduced in the case of citrate or pyrophosphate. Overall, around a 4 times higher phosphate concentration (120 mM) was required to achieve an adequate suppressive effect (Figure 2). The above results prompted us to hypothesize that the anion-dependent control of IL-1ra aggregation could be due to the protein anion interactions at the specific IL-1ra site.

To test this idea, the citrate binding to IL-1ra was assayed as described under Materials and Methods. The system was calibrated with various citrate standards, and the control experiment demonstrated that, in the absence of IL-1ra, no citrate binding was observed under our experimental conditions (Figure 3A). The results of experiments in the presence of IL-1ra and various citrate concentrations revealed a typical saturation curve characteristic of ligand binding (Figure 3A). These data were used to build a Scatchard plot resulting in estimated one citrate binding site and a dissociation constant (K_d^{citr}) of 3.8 mM (Figure 3B). Next, in order to obtain binding constants for phosphate and pyrophosphate, we conducted competition studies as described in Materials and Methods. The dissociation constants were measured similarly to above, but in the presence of a constant amount of citrate containing various concentrations of competitive anion. The resulting apparent K_d^{citr} values for citrate were plotted against the corresponding amounts of unbound (free) competitor (X(f)). Both phosphate and pyrophosphate competed with citrate for the same IL-1ra binding site as judged by an increase in the apparent K_d^{citr} values (Figure 4). The estimated K_d values for phosphate and pyrophosphate were 13.7 mM and 2.9 mM, respectively. The competition data suggested that the phosphate anion had around 4-fold weaker affinity

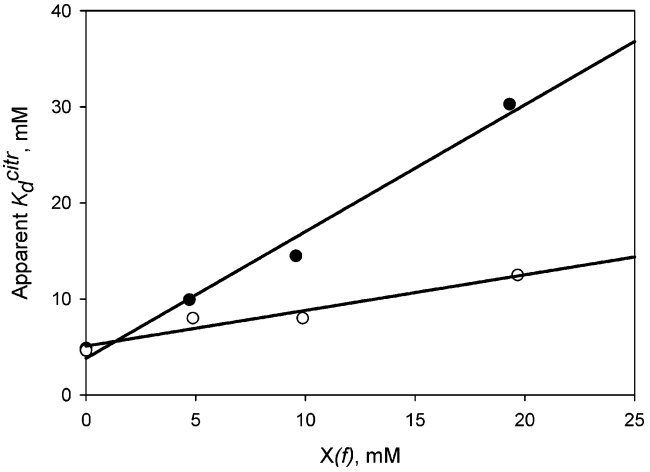

FIGURE 4: Anion competition for the IL-1ra binding site. Apparent K_d values for citrate binding are plotted vs corresponding concentrations of unbound (free) competitive anion (*X*(f)), i.e., pyrophosphate (filled circles) and phosphate (open circles). See Materials and Methods for experimental details.

for the IL-1ra binding site than either citrate or pyrophosphate. The results of anion-dependent aggregation and anion binding experiments were in good agreement and indicated that the anion dependence of IL-1ra aggregation rates could be due to the difference in the strength of protein−anion interactions at the IL-1ra single, positively charged site.

Probing of the IL-1ra Anion Binding Site with Methyl Acetyl Phosphate. Since the above data suggested the existence of a single, positively charged site on IL-1ra in connection with the protein aggregation process, we attempted to locate this site using methyl acetyl phosphate (MAP). MAP is a small dual-mode (anionic and reactive) affinity probe (Figure 5A, inset) that has been previously employed to acetylate nucleophilic amino groups within protein anion binding sites (*23*−*25*). The reaction of IL-1ra with MAP in 10 mM citrate buffer, pH 6.5 was monitored by reverse-phase HPLC during a 5.5 h incubation at 37 °C as described under Materials and Methods and resulted in the shift of the main peak along with the simultaneous appearance of another three major peaks (Figure 5A). This was suggestive of protein being modified at least at four different reactive sites during its incubation with MAP. In order to see if this was an anion dependent reaction, i.e., both anion and anionic probe can act as competitors for the above-mentioned reactive site(s), the experiment was repeated and data were analyzed using the same conditions with the exception of citrate being replaced with either phosphate or pyrophosphate. The chromatography data comparison revealed similar peak profiles indicating on the same reactive sites involved in the presence of different anions (Figure 5B). On the other hand, there was a visible anionic effect on the extent of MAP reaction with IL-1ra, i.e., the largest extent of modification was observed in the presence of phosphate followed by citrate and pyrophosphate suggesting that phosphate and pyrophosphate were the least and the most competitive anions for the MAP-reactive sites of IL-1ra, respectively. Interestingly, when the same experiment was conducted at the slightly higher pH 6.7, the pyrophosphate became less competitive as its MAP reaction profile shifted to resemble that of the citrate (data not shown). In the next step, we attempted to identify the IL-1ra

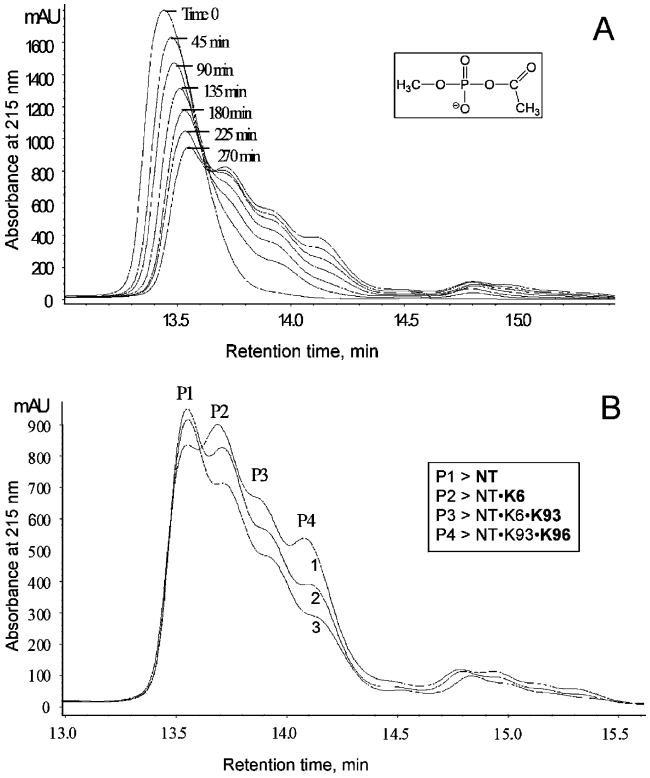

FIGURE 5: Reverse-phase HPLC analysis of IL-1ra modification with MAP at 37 °C and pH 6.5. (A) Time course of reaction as monitored by HPLC during 4.5 h incubation of IL-1ra with 10-fold excess of MAP. The structure drawing of MAP is shown in the inset. (B) Comparative HPLC profiles obtained at 5.5 h time point of MAP reaction in the presence of phosphate (curve 1), citrate (curve 2), and pyrophosphate (curve 3). Inset shows protein MAP-derived modification sites identified in the four major peaks P1−P4.

modification sites associated with the appearance of the four weakly resolved peaks designated as P1, P2, P3, and P4 (Figure 5B). After a 5.5 h reaction with MAP in 10 mM citrate buffer, pH 6.5, the reaction products were separated on the reverse-phase C18 HPLC column, the peak-associated fractions were collected and digested with endoproteinase Lys-C, and the resulting digests were subjected to mass spectral analysis (see Materials and Methods for details). Each reactive site was determined by the presence of an additional acetyl group on a peptide that, in turn, was judged by an increase of 42 *m*/*z* on the MS profile relative to unmodified peptide present in the control digest (data not shown). A total of four different modification site residues were identified as NT (N-terminal), K6, K93, and K96 (Figure 5B). It should be noted that, due to the low peak resolution, a certain overlap in modification sites was observed in adjacent peak fractions, however, it did not interfere with the overall quality of the mass spectral data. The recombinant IL-1ra used in this study contained an extra methionine at its N-termini, which was one of the four MAP-reactive sites. The other three reactive residues (K6, K93, and K96) were assigned according to the original sequence of IL-1ra, where the extra methionine-1 was omitted for clarity. The fact that, out of all four, three sites belonged to lysine residues (protein has total of nine lysines) that displayed an anion-dependent reactive pattern suggested K6, K93, and K96 contribution to the IL-1ra positively charged

surface cluster(s). According to the previous IL-1ra structural studies, the protein twelve β-strands are connected by eleven loops. K93 and K96 plus another two charged residues, R92 and R97, are located on the large loop 84−98, containing a short 3_{10} helical region (*17*−*19*). Remarkably, the electrostatic surface calculations of IL-1ra performed earlier by Oldfield and co-workers (*26*) suggested the existence of the positively charged cluster as a sum contribution from the above loop 84−98 and the unstructured N-terminal region which, in this case, would include K6.

Effect of Mutagenesis of Lysine-93 and N-Terminal Truncation on IL-1ra Aggregation Properties. The likely involvement of the positively charged cluster in anion-dependent protein aggregation led us to investigate specifically the contribution of the K93 residue (see also Discussion on the role of K93) and the unstructured N-terminal region of IL-1ra.

First, lysine-93 was changed to alanine by PCR-based mutagenesis as described in Materials and Methods. The choice of alanine residue was driven by the fact it was earlier reported as a "neutral" mutation that had no effect on IL-1ra functional properties (*27*). The recombinant K93A IL-1ra was expressed in *E. coli*, purified to yield about 4 mg/g cell paste, and was about 98% pure as judged by SDS−PAGE analysis. The mutated protein displayed properties of the wild-type IL-1ra based on the SDS−PAGE, size-exclusion chromatography, circular dichroism, and functional (IL-1 receptor binding and cell-based) analyses (data not shown). However, contrary to the wild-type IL-1ra, the thermally induced aggregation of mutated protein was dramatically suppressed. No aggregation was observed for K93A IL-1ra whereas, under the same conditions, wild-type protein aggregated within the first 2 h of incubation (Figure 6A). The data revealed an important role for lysine-93 of the loop 84−98 in IL-1ra aggregation at elevated temperature.

Second, the protein was N-terminally truncated by limited proteolysis with endoproteinase Lys-C as described in Materials and Methods. The digestion was followed by reverse-phase HPLC analysis that showed a retention time shift for the main protein peak with the simultaneous appearance of the earlier eluted new peak. The nearly complete conversion of the protein native peak into the above two peaks was observed after 48 h proteolysis at 37 °C. Both peaks were isolated and identified. The new peak was identified by mass spectrometry and belonged to a protein N-terminal peptide $(M)^1$RPSGRK^6, whereas the second (shifted main) peak revealed N-terminal amino acid sequence (first 10 residues) of ^{7}SSKMQAFRIW^{16}. Thus, under our experimental conditions, the unstructured N-terminal fragment $(M)^1$RPSGRK^6 of IL-1ra was effectively clipped off the protein. In the next step, the truncated protein was compared at the same conditions with the wild-type IL-1ra in the aggregation assay. The results presented in Figure 6B showed an effect of truncation on aggregation kinetics resulting in moderate 2-fold decrease in the aggregation rate. Interestingly, the truncation also resulted in about a 2-fold increase (from 30 min to 1 h) in the lag phase suggesting a contribution of the unstructured N-terminal region to the earlier, nucleation stage of the aggregation process.

The results indicated that the truncated N-terminal region including the K6 residue played a less significant role in the IL-1ra thermally induced aggregation than the K93-containing loop 84−98.

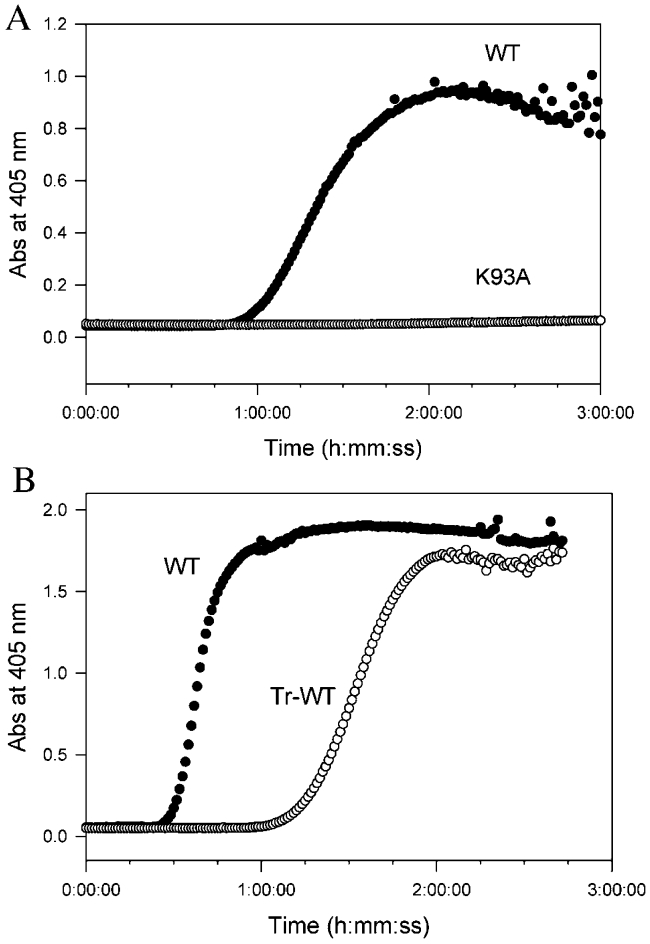

FIGURE 6: Comparative aggregation kinetics of structurally modified IL-1ra. The buffer is 10 mM phosphate, pH 6.5, containing 140 mM NaCl and 0.5 mM EDTA. (A) Mutated (K93A) versus wild type (WT) protein at 100 mg/mL protein concentration. T = 40 °C. (B) Truncated (Tr-WT) versus wild type (WT) protein at 107 mg/mL protein concentration. T = 42 °C.

Effect of Temperature on IL-1ra Native Structure. Since the aggregation of IL-1ra induced by elevated temperature (39 °C−42 °C) could be a result of the thermal perturbation of the protein native structure, we performed a thermal denaturation study combined with circular dichroism (CD) spectral analysis. Thermal denaturation of IL-1ra (0.09 mg/mL) was conducted in 50 mM sodium phosphate buffer, pH 7 containing 0−0.5 M NaCl. Addition of NaCl in the sample buffer solution improved the reversibility of the protein thermal denaturation process. The protein sample solution was gradually heated, cooled, and subsequently reheated within the range of 20°−85 °C while the CD signal data at 230 nm were simultaneously collected. The thermally induced loss of the IL-1ra secondary structure started around 55 °C and was complete around 70 °C as manifested by an increase in the negative ellipticity associated with protein unfolding (Figure 7). The thermal denaturation of IL-1ra was a reversible process, since most of the signal was recovered upon the cooling step. The somewhat lower signal recovery was attributed to a residual protein loss during the preceding heating step. Similar results were obtained when the CD signal was monitored at 281 nm (near-UV region of spectrum), i.e., no changes in the packing of aromatic

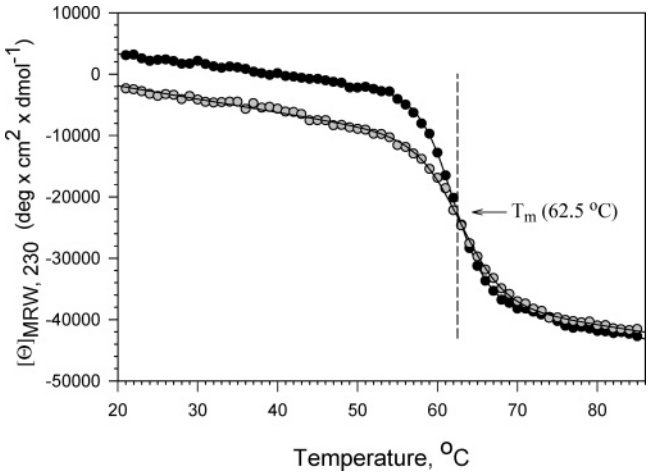

FIGURE 7: The temperature effect on the IL-1ra secondary structure. Sample is 5 μM IL-1ra solution in 50 mM phosphate buffer, pH 7.0 containing 0.5 M NaCl. Circular dichroism measurements are taken at 230 nm. The sample gradual heating (black filled circles) is immediately followed by cooling and then by reheating (gray filled circles) with the same rate of the temperature change. The estimated melting temperature (T_m) is indicated by an arrow.

Table 1: Molecular and IL-1ra-Binding Properties of Anions

anion	distance between ionized groups, Å	pK at 25 °C[a]	K_d (IL-1ra), mM
phosphate (PO_4^{3-})	2.8	2.15, 7.20, 12.35	13.7
citrate ($C_6H_5O_7^{3-}$)	5.9 (min) 6.9 (max)	3.13, 4.76, 6.34	3.8
pyrophosphate ($P_2O_7^{4-}$)	2.5 (min) 5.5 (max)	0.83, 2.26, 6.72, 9.46	2.9

[a] Reference *29*.

residues were detected up to 55 °C (data not shown). The melting temperature (T_m) of IL-1ra estimated as 62.5 °C was far above the temperature used in the aggregation studies. The apparent T_m value of 56 °C has been previously obtained for IL-1ra under irreversible (due to protein precipitation) conditions using differential scanning calorimetry (*28*). Overall, our data did not reveal any perturbations in the IL-1ra structure at temperatures (39°−42 °C) used to induce protein aggregation. They do not, however, exclude a possibility of the protein local conformational changes.

DISCUSSION

What Determines the Strength of Anion−IL-1ra Interactions? As illustrated in the Table 1, the binding properties of the anion can be linked to its ionization state at a given pH (*3*). Citrate, phosphate, and pyrophosphate molecules can have a total of three, three, and four ionized groups, respectively. On the basis of the pK values at 25 °C, the citrate and pyrophosphate at pH 6.5 would have predominantly two/three negatively charged groups, whereas only one ionized group would be prevalent in the case of phosphate. According to the literature (*29*), the higher temperature (39−42 °C) used in our aggregation studies would have little influence over the pK values of citrate and phosphate. The pyrophosphate pK_1 and pK_2 values would be largely unaffected as well; however, the estimated value of pK_3 can be somewhat lower and tend to fluctuate from around 5.8 to 6.8 depending on measurement conditions (*29*). Another factor that may influence the anion binding properties is the size of the molecule and, specifically, the distance between its charged groups (Table 1). To estimate distances, a three-dimensional model of each molecule was built and analyzed using ChemBats3D (Cambridgesoft, Inc.) and Weblab Viewer Lite (Accelrys, Inc.) software packages. Out of all three, the citrate is the largest molecule with the minimal distance value of 5.9 Å, which is close to the maximum distance value of 5.5 Å for pyrophosphate. Therefore, in addition to a similarity in the ionization properties between molecules of citrate and pyrophosphate, a commonly featured 5−6 Å distance between their charged groups can help to explain a similar behavior of these molecules during the IL-1ra binding and aggregation experiments. In the case of phosphate, a weaker binding to IL-1ra can also be attributed to the ionization factor (single ionized group at pH 6.5), whereas the distance factor between charged groups presumably would have a minor or no impact.

How Could IL-1ra Aggregation Be Affected by Anion Binding? Our data suggest that anions affect IL-1ra aggregation via interactions with the protein single, positively charged site. As already mentioned in Results, this site can be assembled from the highly charged loop 84−98 (residues R92, K93, K96, R97) and, perhaps, a disordered and also charged N-terminal region 1−7 (residues R1, R5, K6). There is no crystal structure information available to date with respect to the highly mobile N-terminal region 1−7, so our further discussion will be focused primarily on the loop 84−98 as defined by the IL-1ra crystal structure previously reported by Schreuder et al. (*19*). First of all, despite the fact that IL-1ra is a monomeric protein in solution, its crystal cell unit contains two protein molecules positioned such that they would form an asymmetric "dimer" where loop 84−98 of one molecule (chain 2) is placed at the "dimer" interface. The closer inspection of the interface region revealed that K93 and R97 residues of chain 2 are in close proximity with corresponding W16 and Y34 residues of chain1, suggesting that they may form cation−π interactions (Figure 8A) (*30*, *31*). Indeed, the energetically significant cation−π interactions between the above residue pairs were identified by the CaPTURE program (*31*) using IL-1ra structural data file 1ILR.pdb. Second, the crystal structure points to an altered position of K93 of chain 2 at the "dimer" interface. The estimated distance between the side chain groups of K93 and K96 at the interface region (11.5 Å) is about twice as long as the distance between the same pair of residues of chain 1 (5.4 Å), suggesting a rearrangement of the K93 side chain group of chain 2 to permit a contact with an aromatic ring of W16 of chain 1 (Figure 8B). In contrast to the crystallographic data, a three-dimensional NMR spectroscopy study of IL-1ra in solution by Stockman et al. (*32*) failed to define the K93−Q94 region (K94−Q95 in their study) of the loop 84−98, pointing to this region's highly dynamic nature. Thus, the loop 84−98 ordering via cation−π interactions between two or even more protein molecules and, therefore, their asymmetric association may be required to permit nucleation and subsequent crystal growth. This, in turn, would lead us to a potential existence of the certain equilibrium in IL-1ra solution between monomeric and oligomeric species. Assuming that, in solution, the same positively charged site could be involved in formation of either protein−anion or protein intermolecular cation−π

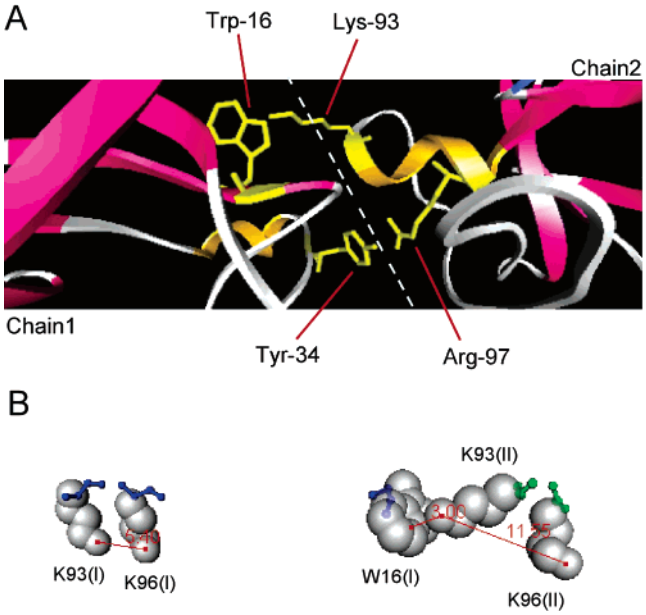

FIGURE 8: IL-1ra crystal structure (*19*) points to an involvement of the cationic region in the protein self-association. The structure was drawn using the PDB coordinate file 1ILR. (A) shows a fragment of the "dimer" interface (dotted line) where K93 and R97 of the polypeptide chain 2 are positioned against W16 and Y34 of chain 1, respectively, to form cation−π interactions (see Discussion for details). (B) Illustration of the rearrangement of K93 (II) toward W16 (I) with corresponding increase in the distance between K93 (II) and K96 (II). Chain number is shown in brackets. The side chains of the specified residues and their distances are shown while the rest of the structure is omitted for clarity.

interactions, the addition of a competitive anion would shift equilibrium toward the IL-1ra monomer. Previous studies indicate that both protein aggregation and crystallization are nucleation-dependent kinetic processes that could be intrinsically linked at the early stage preceding the nucleus formation (*33*−*35*). On the other hand, the IL-1ra aggregation with its characteristic sigmoidal curve and pronounced lag phase resembles a crystallization process and is consistent with the amyloid nucleation-dependent polymerization model where the stable nucleus formation is the rate-limiting step (*36*−*38*).

On the basis of all of the above, it is reasonable to suggest that the IL-1ra positively charged site contributed by loop 84−98 is involved in the protein asymmetric self-association that could play an important role at the initial, perhaps nucleation stage of the protein aggregation process. Consequently, anion interaction with the IL-1ra positively charged site would control/suppress protein aggregation via interference with its self-association pathway.

ACKNOWLEDGMENT

Many thanks to Songpon Deechongkit, who helped to estimate distances between anion charge groups, and David Brems for useful discussions throughout the course of this study.

REFERENCES

1. Horwich, A. (2002) Protein aggregation in disease: a role for folding intermediates forming specific multimeric interactions, *J. Clin. Invest. 110*, 1221−1232.
2. Burgess, W. H. and Maciag, T. (1989) The heparin-binding (fibroblast) growth factor family of proteins, *Annu. Rev. Biochem. 58*, 575−606.
3. Chen, B. L., Arakawa, T., Morris, C. F., Kenney, W. C., Wells, C. M., and Pitt, C. G. (1994) Aggregation pathway of recombinant human keratinocyte growth factor and its stabilization, *Pharm. Res. 11*, 1581−1587.
4. Volkin, D. B., Tsai, P. K., Dabora, J. M., Gress, J. O., Burke, C. J., Linhardt, R. J., and Middaugh, C. R. (1993) Physical stabilization of acidic fibroblast growth factor by polyanions, *Arch. Biochem. Biophys. 300*, 30−41.
5. Kajio, T., Kawahara, K., and Kato, K. (1992) Stabilization of basic fibroblast growth factor with dextran sulfate, *FEBS Lett. 306*, 243−246.
6. Conway, K. A., Harper, J. D., and Lansbury, P. T., Jr. (2000) Fibrils formed in vitro from α-synuclein and two mutant forms linked to Parkinson's disease are typical amyloid, *Biochemistry 39*, 2552−2563.
7. Serpell, L. C., Berriman, J., Jakes, R., Goedert, M., and Crowther, R. A. (2000) Fiber diffraction of synthetic alfa-synuclein filaments shows amyloid-like cross-beta conformation, *Proc. Natl. Acad. Sci. U.S.A. 97*, 4897−4902.
8. Fandrich, M., Fletcher, M. A., and Dobson, C. M. (2001) Amyloid fibrils from muscle myoglobin, *Nature 410*, 165−166.
9. Patro, S. Y., and Przybycien, T. M. (1996) Simulations of reversible protein aggregate and crystal structure, *Biophys. J. 70*, 2888−2902.
10. Ferrone, F. (1999) Analysis of protein aggregation kinetics, *Methods Enzymol. 309*, 256−274.
11. Chiti, F., Taddei, N., Baroni, F., Capanni, C., Stefani, M., Ramponi, G., and Dobson, C. M. (2002) Kinetic partitioning of protein folding and aggregation, *Nat. Struct. Biol. 9*, 137−143.
12. Uversky, V. N., Li, J., and Fink, A. L. (2001) Metal-triggered structural transformations, aggregation, and fibrillation of human alfa-synuclein. A possible molecular NK between Parkinson's disease and heavy metal exposure, *J. Biol. Chem. 276*, 44284−44296.
13. Kurganov, B. I., Rafikova, E. R., and Dobrov, E. N. (2002) Kinetics of thermal aggregation of tobacco mosaic virus coat protein, *Biochemistry (Moscow) 67*, 525−533.
14. Maclean, D. S., Qian, Q., and Middaugh, C. R. (2002) Stabilization of proteins by low molecular weight multi-ions, *J. Pharm. Sci. 91*, 2220−2229.
15. Arend, W. P. (2002) The balance between IL-1 and IL-1ra in disease, *Cytokine Growth Factor Rev. 13*, 323−340.
16. Murzin, A. G., Lesk, A. M., and Chothia, C. (1992) beta-Trefoil fold. Patterns of structure and sequence in the Kunitz inhibitors interleukins-1 beta and 1 alpha and fibroblast growth factors, *J. Mol. Biol. 223*, 531−543.
17. Vigers, G. P. A., Caffes, P., Evans, R. J., Thompson, R. C., Eisenberg, S. P., and Brandhuber, B. J. (1994) X-ray structure of interleukin-1 receptor antagonist at 2.0-A resolution, *J. Biol. Chem. 269*, 12874−12879.
18. Stockman, B. J., Scahill, T. A., Strakalaitis, N. A., Brunner, D. P., Yem, A. W., and Deibel, M. R., Jr. (1994) Solution structure of human interleukin-1 receptor antagonist protein, *FEBS Lett. 349*, 79−83.
19. Schreuder, H. A., Rondeau, J. M., Tardif, C., Soffientini, A., Sarubbi, E., Akeson, A., Bowlin, T. L., Yanofsky, S., and Barrett, R. W. (1995) Refined crystal structure of the interleukin-1 receptor antagonist. Presence of a disulfide link and a cis-proline, *Eur. J. Biochem. 227*, 838−847.
20. Stinson, R. A., and Holbrook, J. J. (1973) Equilibrium binding of nicotinamide nucleotides to lactate dehydrogenases, *Biochem. J. 131*, 719−728.
21. Kluger, R., and Tsui, W. C. (1980) Methyl acetyl phosphate. A small anionic acetylating agent, *J. Org. Chem. 45*, 2723−2724.
22. Horton, R. M., Cai, Z. L., Ho, S. N., and Pease, L. R. (1990) Gene splicing by overlap extension: tailor-made genes using the polymerase chain reaction, *Biotechniques 8*, 528−535.
23. Kluger, R, and Tsui, W. C. (1986) Reaction of the anionic acetylation agent methyl acetyl phosphate with D-3-hydroxybutyrate dehydrogenase, *Biochem. Cell Biol. 64*, 434−440.
24. Ueno, H., Pospischil, M. A., and Manning, J. M. (1989) Methyl acetyl phosphate as a covalent probe for anion-binding sites in human and bovine hemoglobins, *J. Biol. Chem. 264*, 12344−12351.
25. Kataoka, K., Tanizawa, K., Fukui, T., Ueno, H., Yoshimura, T., Esaki, N., and Soda, K. (1994) Identification of active site lysyl residues of phenylalanine dehydrogenase by chemical modification with methyl acetyl phosphate combined with site-directed mutagenesis, *J. Biochem. (Tokyo) 116*, 1370−1376.

26. Oldfield, T. J., Murray-Rust, P., and Hubbard, R. E. (1993) Model structures and action of interleukin 1 and its antagonist, *Protein Eng. 6*, 865−871.
27. Evans, R. J., Bray, J., Childs, J. D., Vigers, G. P. A., Brandhuber, B. J., Skalicky, J. J., Thompson, R. C., and Eisenberg, S. P. (1995) Mapping receptor binding sites in interleukin (IL)-1 receptor antagonist and IL-1β by site-directed mutagenesis, *J. Biol. Chem. 270*, 11477−11483.
28. Zhang, Y., Roy, S., Jones, L. S., Krishnan, S., Kerwin, B. A., Chang, B. S., Manning, M. C., Randolph, T. W., and Carpenter, J. F. (2004) Mechanism for benzyl alcohol-induced aggregation of recombinant human interleukin-1 receptor antagonist in aqueous solution, *J. Pharm. Sci. 93*, 3076−3089.
29. Goldberg, R. N., Kishore, N., and Lennen, R. M. (2002) Thermodynamic quantities for the ionization reactions of buffers, *J. Phys. Chem. Ref. Data 31*, 231−370.
30. Dougherty, D. A. (1996) Cation-pi interactions in chemistry and biology: a new view of benzene, Phe, Tyr, and Trp, *Science 271*, 163−168.
31. Gallivan, J. P., and Dougherty, D. A. (1999) Cation-pi interactions in structural biology, *Proc. Natl.* Acad. *Sci. U.S.A. 96*, 9459−9464.
32. Stockman, B. J., Scahill, T. A., Roy, M., Ulrich, E. L., Strakalaitis, N. A., Brunner, D. P., Yem, A. W., and Deibel, M. R., Jr. (1992) Secondary structure and topology of interleukin-1 receptor antagonist protein determined by heteronuclear three-dimensional NMR spectroscopy, *Biochemistry 31*, 5237−5245.
33. McPherson, A. (1999) Some Physical and Energetic Principles, in *Crystallization of Biological Macromolecules*, pp 127−158, Cold Spring Harbor Laboratory Press, New York.
34. Stura, E. A., Martin, L., Lortat-Jacob, H., Vives, R., and Vita, C. (2002) Heparin-aggregated RANTES can be crystallised, *Acta Crystallogr., Sect. D: Biol. Crystallogr. 58*, 1670−1673.
35. Schuler, J., Frank, J., Saenger, W., and Georgalis, Y. (1999) Thermally induced aggregation of human transferrin receptor studied by light-scattering techniques, *Biophys. J. 77*, 1117−1125.
36. Jarrett, J. T., and Lansbury, P. T., Jr. (1992) Amyloid fibril formation requires a chemically discriminating nucleation event: studies of an amyloidogenic sequence from the bacterial protein OsmB, *Biochemistry 31*, 12345−12352.
37. Jarrett, J. T., Berger, E. P., and Lansbury, P. T., Jr. (1993) The carboxy terminus of the β amyloid protein is critical for the seeding of amyloid formation: implications for the pathogenesis of Alzheimer's disease, *Biochemistry 32*, 4693−4697.
38. Come, J. H., Fraser, P. E., and Lansbury, P. T., Jr. (1993) A kinetic model for amyloid formation in the prion diseases: importance of seeding, *Proc. Natl. Acad. Sci. U.S.A. 90*, 5959−5963.

BI050388G